Supporting Information

Estimation of K_D values for octapeptide binding to states B and C of C34 WT

Consider the model of Figure 2d where A denotes the octapeptide-bound state of C34 WT and B and C are the interconverting *apo* states. We can write

$$K_D^{AB} = \frac{[B]\cdot[L]}{[A]},\ K_D^{AC} = \frac{[C]\cdot[L]}{[A]},\ K^{CB} = \frac{[C]}{[B]}. \quad [S1]$$

Since states B and C are significantly populated in the WT protein and for the reporter peaks used in the NMR analysis of affinities $\Delta\varpi_{BC}$ ~ 0 ppm (Fig. 5a), the apparent peptide binding affinity is given by

$$K_D^{app} = \frac{([B]+[C])\cdot[L]}{[A]} = K_D^{AB} + K_D^{AC} = K_D^{AB}\cdot\left(1 + K^{CB}\right) = K_D^{AC}\cdot\left(1 + \frac{1}{K^{CB}}\right), \quad [S2]$$

from which we can write,

$$K_D^{AB} = K_D^{app}\cdot\frac{1}{1+K^{CB}},\ K_D^{AC} = K_D^{app}\cdot\frac{K^{CB}}{1+K^{CB}}. \quad [S3]$$

Using the fitted values for the WT protein of K_D^{app} = 230 μM and K^{CB} = 0.6 (although the χ^2 surface in *SI Appendix*, Fig. S4d indicates that there is significant uncertainty in K^{CB} and that values between 0.3 - 2 are plausible), the calculated values for K_D^{AB} and K_D^{AC} are 140 and 90 μM,

respectively. All the mutations considered in this study (Δβ4, E119V, E124RE) are in the β4 stretch and therefore should not affect the equilibrium between the bound state (state A) and FC1, but only stabilize/destabilize FC2 (Fig. 4c). With the further assumption that FC1 ≡ C, then $K_D^{AC} = K_D^{\Delta\beta4}$= 90 μM, and K_D^{AC} would be invariant to the E119V and E124RE mutations. This calculated value is slightly larger than the measured $K_D^{\Delta\beta4} = 60$ μM. Regarding the two β4-stabilizing mutants, E119V and E124RE, calculations using Eq. S2 indicate that K^{CB} must decrease to about 0.01 and 0.3, respectively, to explain the measured K_D^{app} values.

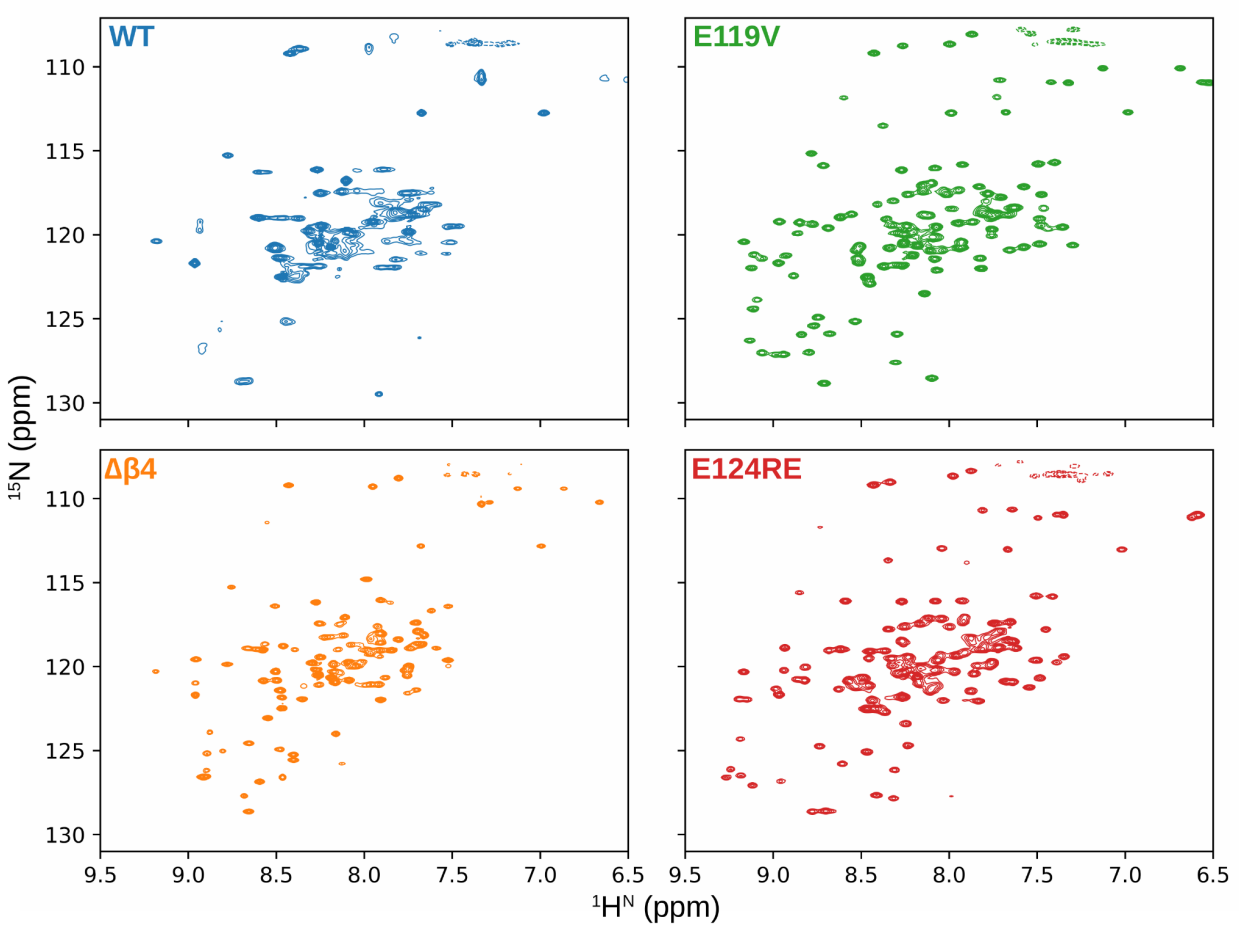

Figure S1. $^{1}H^{N}$-^{15}N HSQC spectra of apo C34 variants recorded at 25°C, 14.1 T. The threshold value for plotting contour levels for the wild-type (WT) spectrum is two-fold lower than for the other three variants.

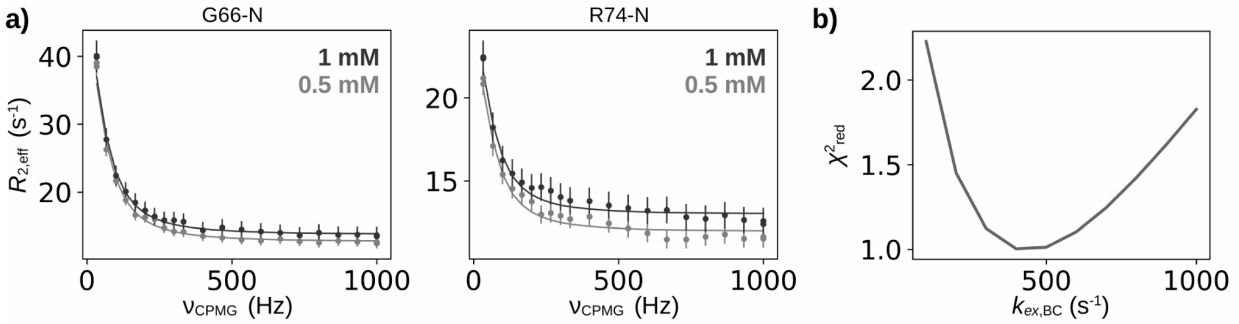

Figure S2. Fits of ^{15}N CPMG data recorded on *apo* C34 WT, 25ºC, 14.1 T. a) ^{15}N CPMG profiles (circles) for G66 and R74 at two different protein concentrations were fit to a two-site exchange model (solid lines). Further fits are shown in Figure 2b. b) 1D plot of reduced χ^2 values *vs* $k_{ex,BC} = k_{BC} + k_{CB}$, corresponding to the exchange rate between WT *apo* states B and C.

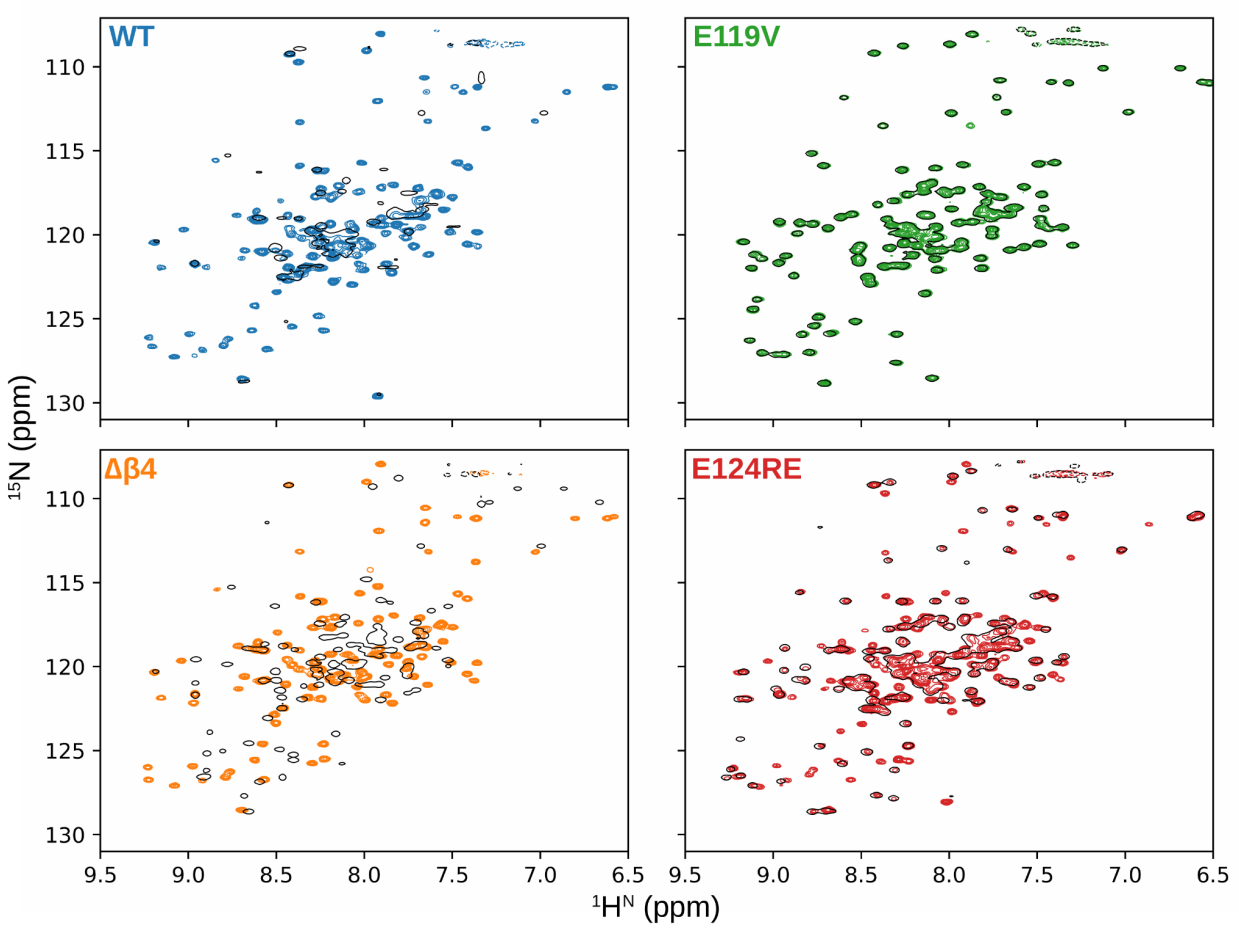

Figure S3. $^{1}H^{N}$-^{15}N HSQC spectra of C34 variants recorded in the presence of a 10-fold excess concentration of octapeptide (colored contours) overlaid with corresponding spectra of the *apo* states of the proteins (single black contours). Spectra were recorded at 25°C, 14.1 T.

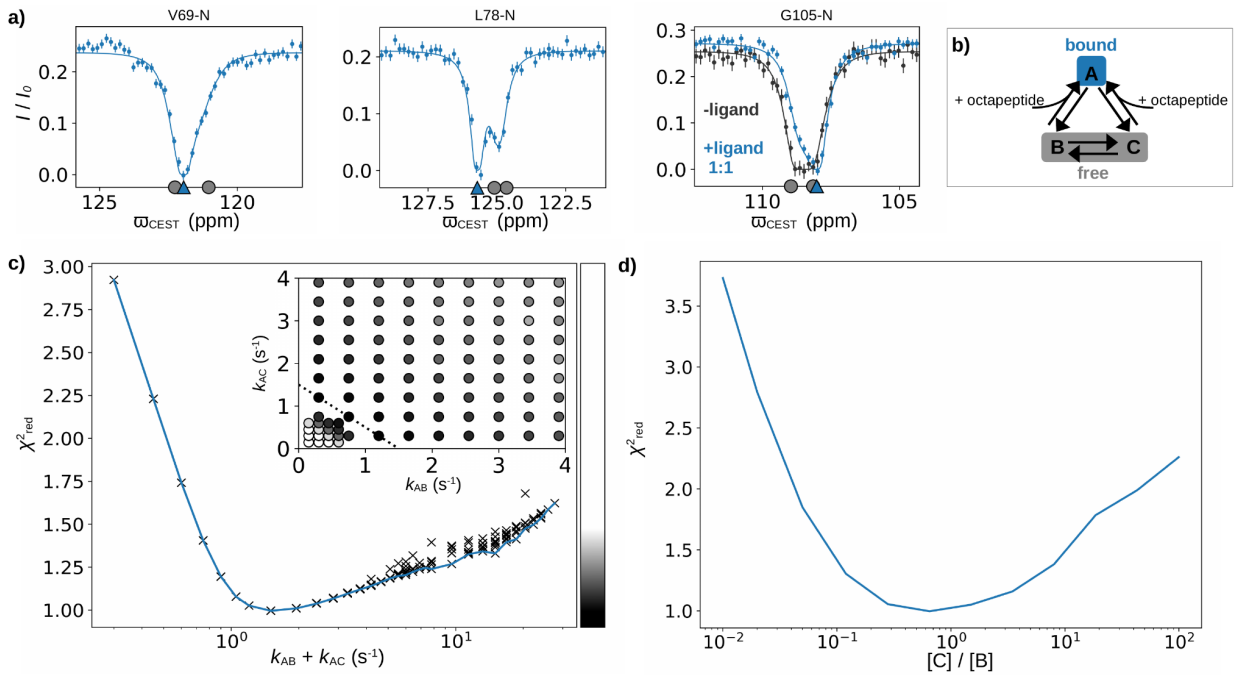

Figure S4. Fits of CEST profiles recorded on a sample of 1:1 (450 μM) C34 WT:peptide, 25°C, to a three-site exchange model. a) Additional ^{15}N CEST profiles, as in Figure 2c. Gray circles on the *x*-axis indicate the fitted values of the chemical shifts for nuclei from the *apo* states, while the shifts of the corresponding nuclei of the bound conformation are shown with blue triangles. b) Three-state model used to fit the data. c) 1D plot of reduced χ^2 values from combined fits of the CEST and CPMG data *vs* the sum of the dissociation rates from states A (octapeptide bound) to B and C (*apo* states). There are multiple "X" for a given *x* position (*ie*, value of k_{AB} +k_{AC}) because there are many degenerate (k_{AB}, k_{AC}) pairs that give the same sum; the minimum χ^2 value is shown by the blue line. The difference in χ^2 between these degenerate combinations is small so that the data doesn't allow the quantification of the relative fluxes from A to B or A to C. (Inset) 2D surface showing reduced χ^2 *vs* (k_{AB}, k_{AC}), colored according to the gray scale shown on the right of the main panel. The dotted line connects the three points with a sum equal to 1.5 s^{-1}, corresponding to the minimum in χ^2. d) 1D plot of reduced χ^2 *vs* K^{CB}, corresponding to the ratio of the populations of *apo* C34 WT states C and B.

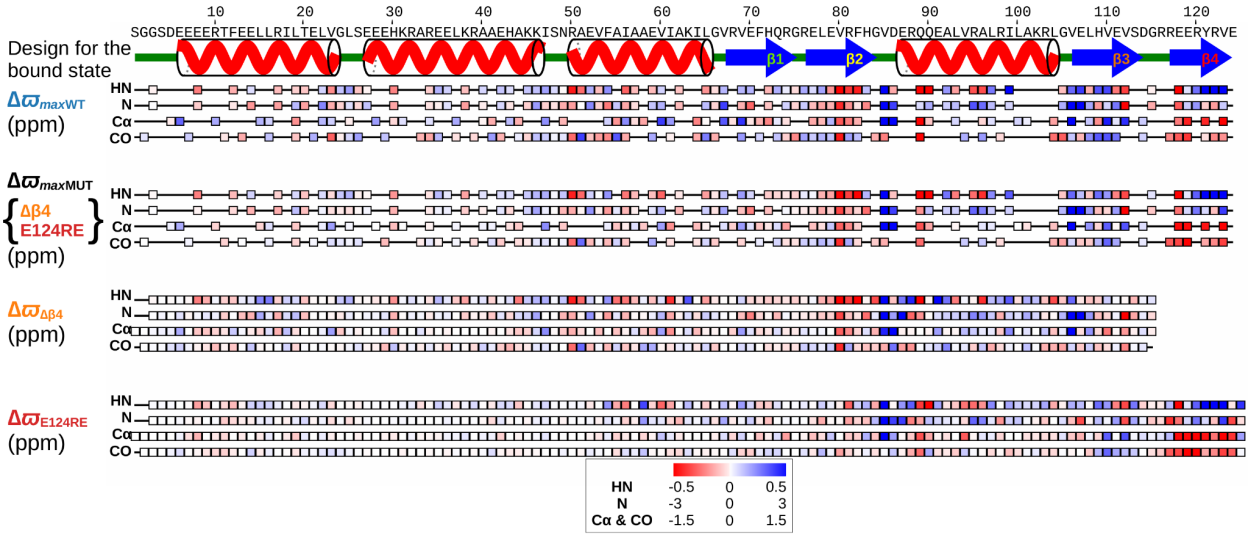

Figure S5. Structural insights into the interconverting states of *apo* C34 WT using mutagenesis. Differences in chemical shifts (ppm) between *apo* and bound states of C34 WT, $\Delta\varpi_{max\mathrm{WT}} = max(\Delta\varpi_{\mathrm{AB}},\Delta\varpi_{\mathrm{AC}})$ obtained from analysis of CEST data, and between *apo* and bound states for variants of C34, $\Delta\varpi_{max\mathrm{MUT}} = max\{\Delta\varpi_{\mathrm{E124RE}},\Delta\varpi_{\Delta\beta4}\}$, calculated from $\Delta\varpi = \varpi_{apo} - \varpi_{peptide\text{-}bound}$ for C34 Δβ4 ($\Delta\varpi_{\Delta\beta4}$), and C34 E124RE ($\Delta\varpi_{\mathrm{E124RE}}$). All nuclei for which data are available are shown in panels for $\Delta\varpi_{\Delta\beta4}$ and $\Delta\varpi_{\mathrm{E124RE}}$ but only residues for which $\Delta\varpi_{max\mathrm{MUT}}$ values are also present in $\Delta\varpi_{max\mathrm{WT}}$ are indicated in the $\Delta\varpi_{max\mathrm{MUT}}$ panel. The $\Delta\varpi$ values are color coded as indicated at the bottom of the figure.

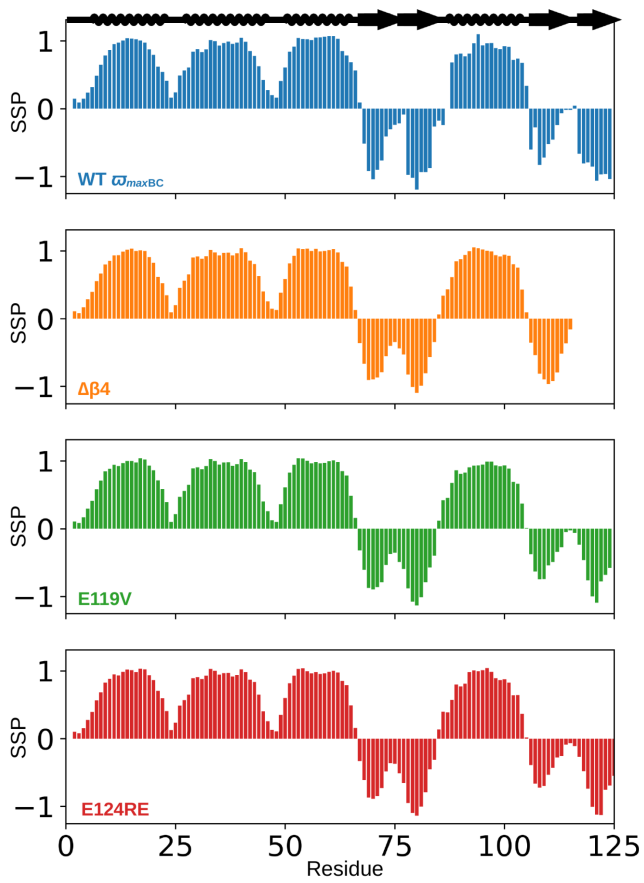

Figure S6. Secondary structure propensity values for four *apo* C34 variants. Positive values indicate α-helical propensity, while negative values indicate β-structure (1). Note that the SSP values for *apo* C34 WT are based on the largest fitted values from CEST, $\Delta\varpi_{maxWT} = max(\Delta\varpi_{AB},\Delta\varpi_{AC})$, so that they report the largest structural deviations from the bound state that occur in either of the two free states.

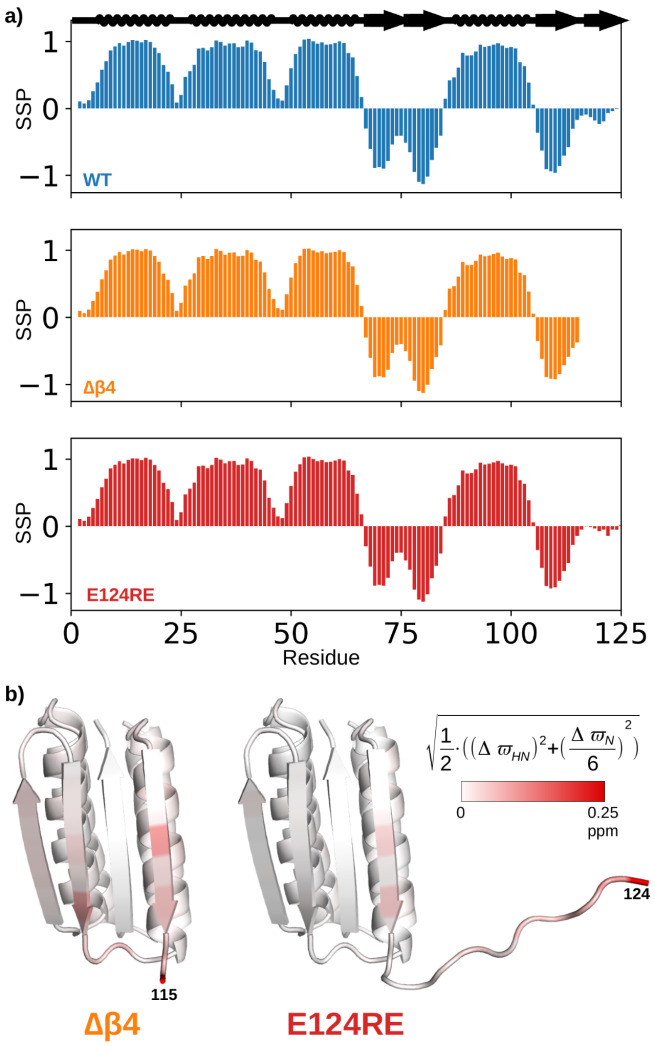

Figure S7. a) Secondary structure propensity values for three C34 variants in the bound state based on assigned backbone chemical shifts of complexes of C34 with octapeptide (assignments at 1:1 C34:octapeptide). b) Combined $\{^{1}H^{N},^{15}N\}$ chemical shift differences (Δβ4 - WT) and (E124RE - WT) for the C34 bound states, showing that all bound conformations are the same. The largest shift differences relative to WT occur at the point of mutation for both C34 Δβ4 and C34 E124RE.

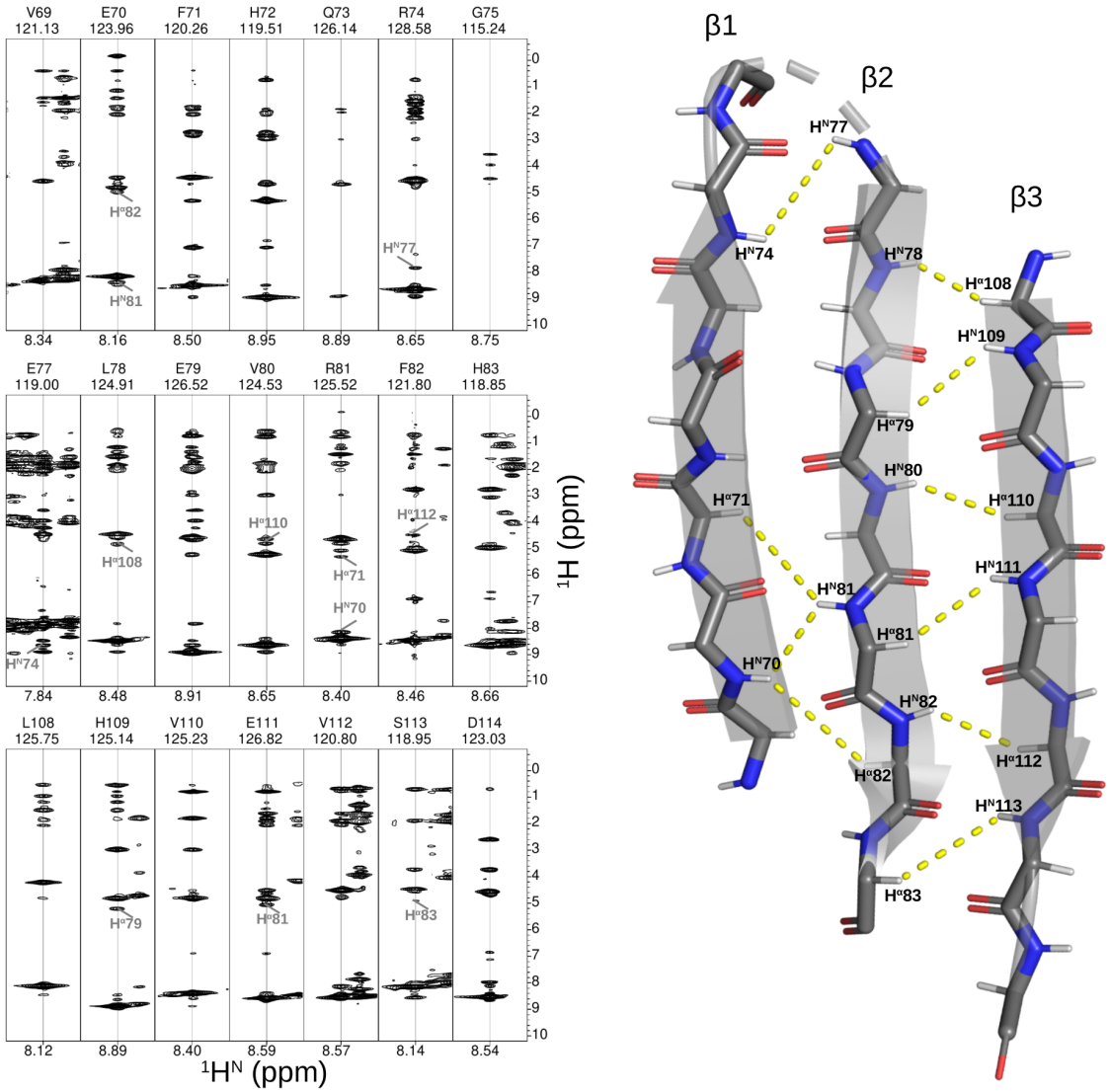

Figure S8. Analysis of NOE contacts for *apo* C34 Δβ4. Strip plots from a 150 ms 3D ^{15}N-edited NOESY spectrum are shown on the left, while NOE contacts are highlighted by dotted lines on the structural model on the right.

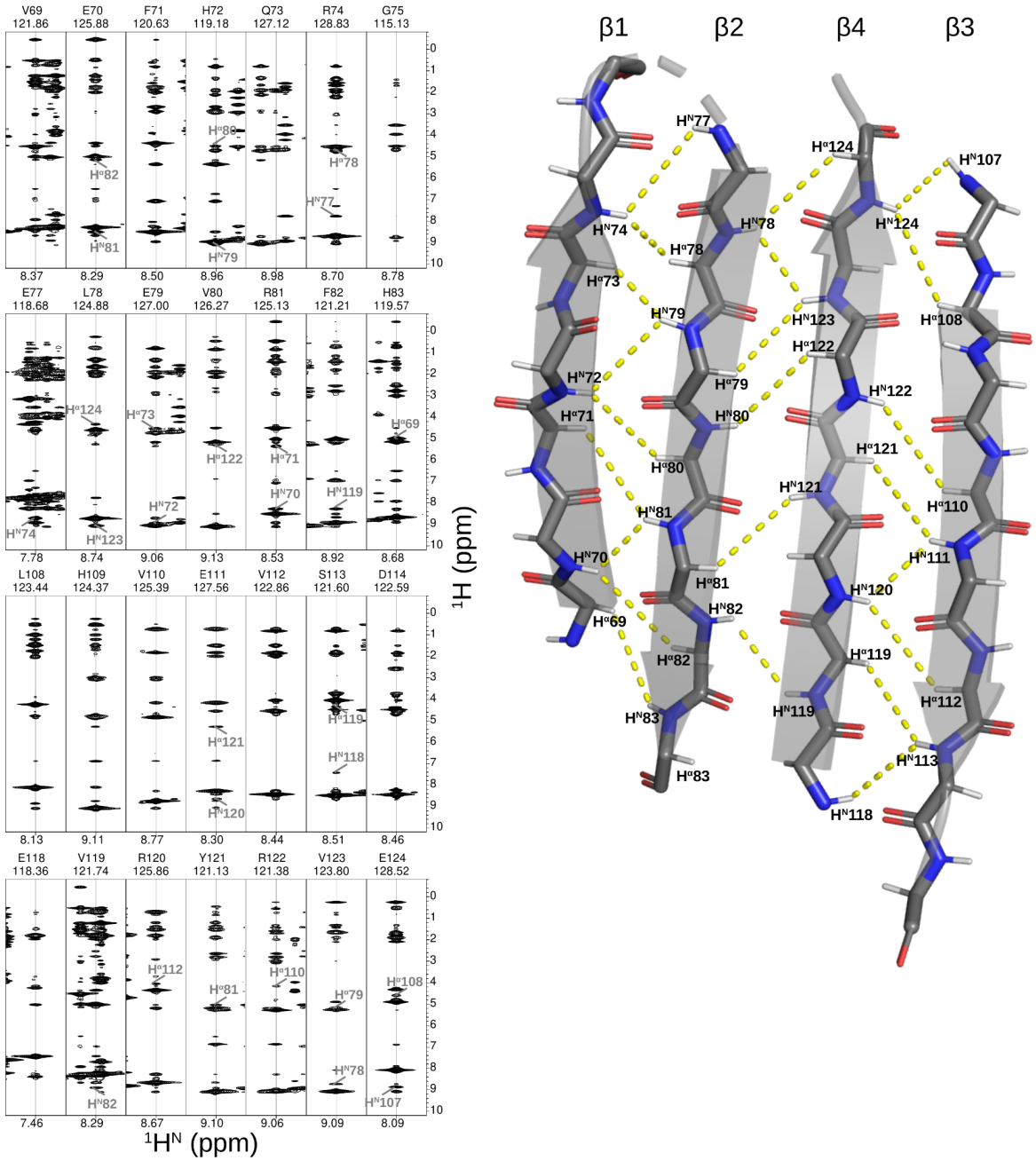

Figure S9. Analysis of NOE contacts for *apo* C34 E119V. Strip plots from a 150 ms 3D ^{15}N-edited NOESY spectrum are shown on the left, while detected NOE contacts are highlighted by dotted lines on the structural model on the right.

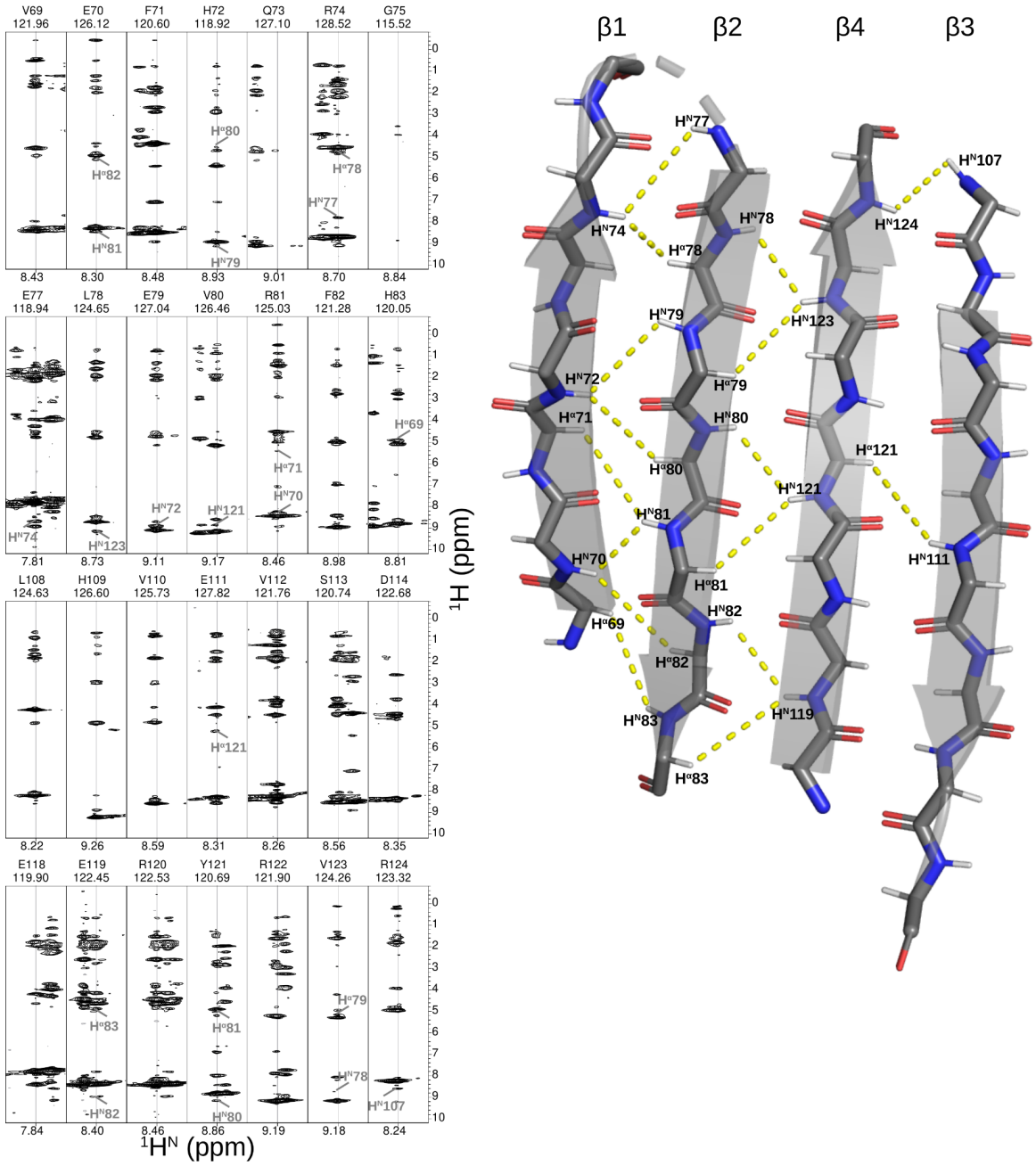

Figure S10. Analysis of NOE contacts for *apo* C34 E124RE. Strip plots from a 150 ms 3D ^{15}N-edited NOESY spectrum are shown on the left, while detected NOE contacts are highlighted by dotted lines on the structural model on the right.

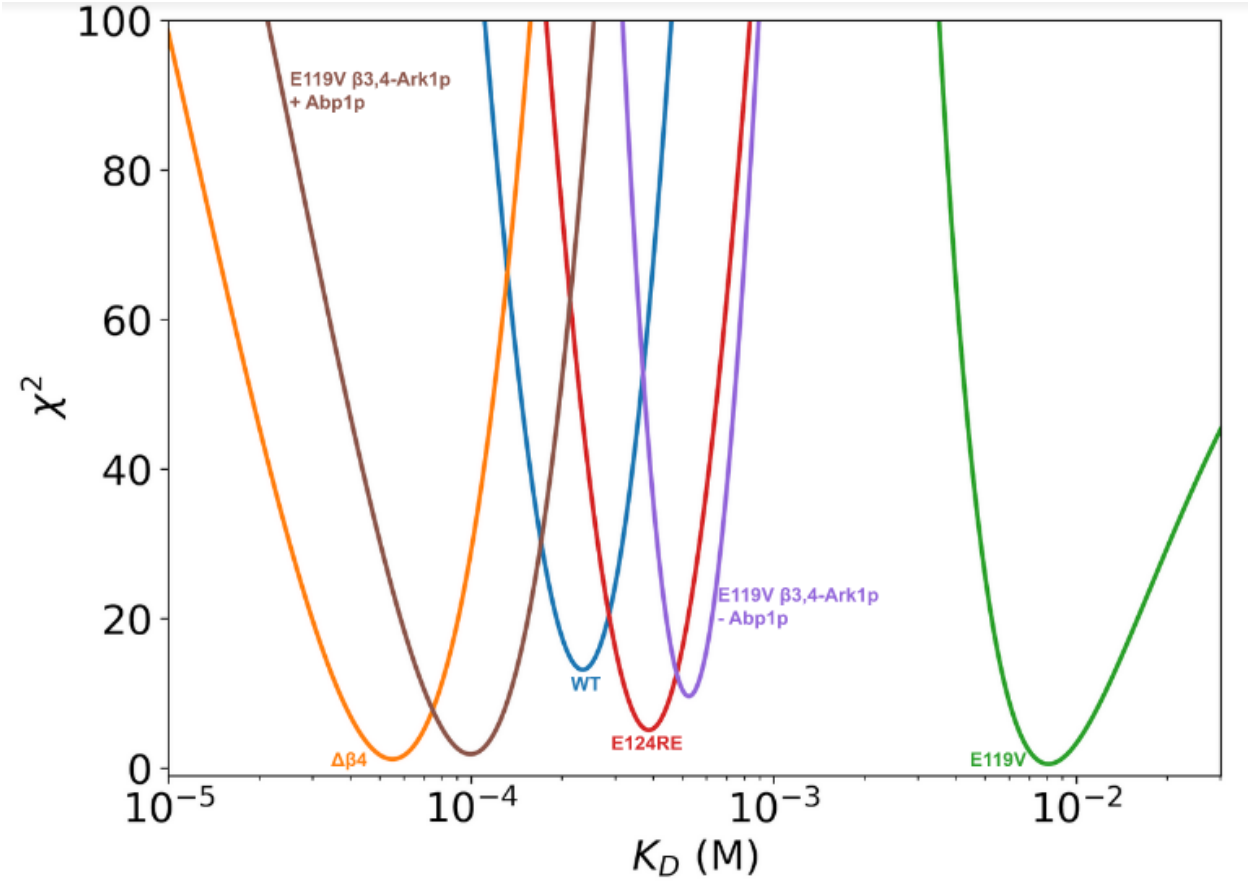

Figure S11. 1D reduced χ^2 plot showing the goodness of fit for K_D values (dissociation constants for octapeptide) for the five C34 variants considered in this work.

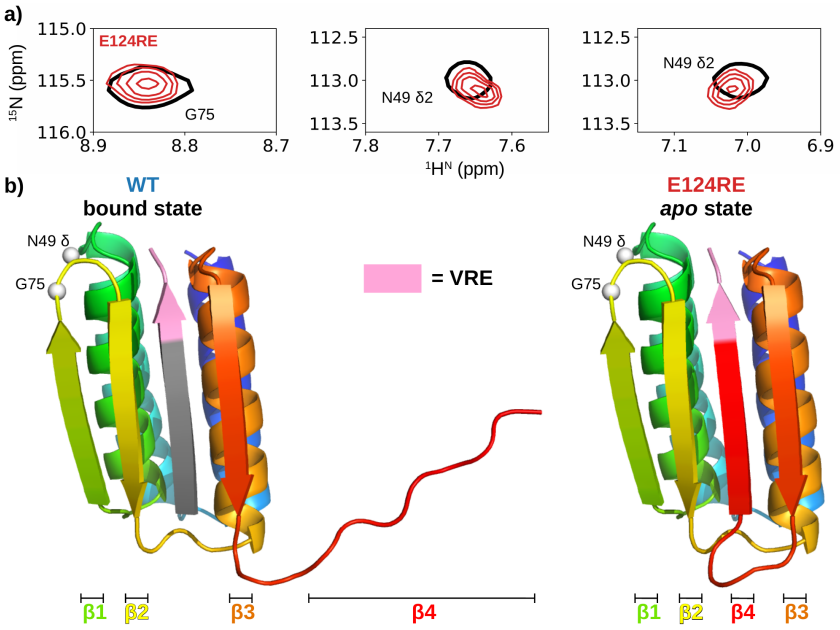

Figure S12. a) $^{1}H^{N}$-^{15}N HSQC spectral regions from datasets of C34 E124RE recorded at 25°C, 14.1T, either without (single black contours) or with added octapeptide at a 1:10 C34:octapeptide ratio. Note that correlations for N49 (sidechain) and G75 change little upon binding of octapeptide, in contrast to what was observed for C34 WT and C34 Δβ4 (Fig. 5a). b) Comparison of structural models of C34 E124RE, peptide bound (left) and *apo* (right), providing insight as to why the depicted peaks shift only slightly upon addition of octapeptide. Both N49 and G75 are relatively close to the C-terminus of either the octapeptide (left) or the mutated β4 strand (right), where the primary sequences of the C-terminal regions of the octapeptide and β4 in the E124RE variant are identical (VRE). For this reason a separate spectral region was highlighted in the C34 E124RE datasets of Figure 5a.

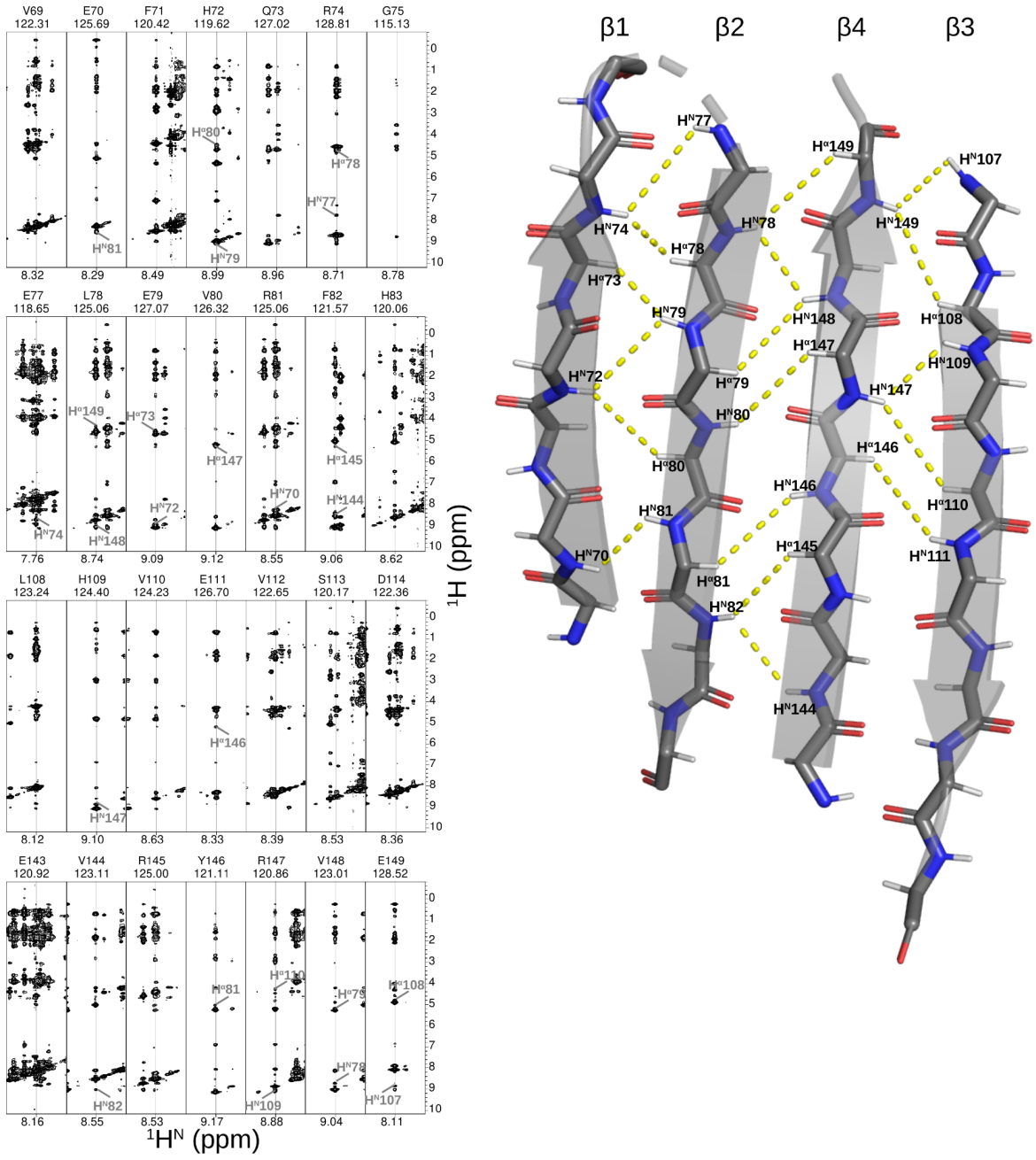

Figure S13. Analysis of NOE contacts for *apo* C34 E119V β3,4-Ark1p. Strip plots from a 150 ms 3D ^{15}N-edited NOESY spectrum are shown on the left, while detected NOE contacts are highlighted by dotted lines on the structural model on the right.

Table S1. Microscopic rates for the three-state models of exchange used to fit CEST data. The two models fit the data equally well.

Model	k_{AB} (s^{-1})	k_{AC} (s^{-1})	k_{BC} (s^{-1})	k_{CB} (s^{-1})
	1.1 ± 0.5	0.4 ± 0.6	155 ± 6	274 ± 4
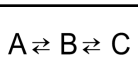	1.5 ± 0.1	0	155 ± 6	274 ± 4

Table S2. Fitted K_D values (μM) for dissociation of octapeptide from the five C34 variants considered in the text.

C34 WT	230 ± 30
C34 Δβ4	55 ± 9
C34 E119V	8100 ± 1200
C34 E124RE	390 ± 40
C34 E119V β3,4-Ark1p - Abp1p	520 ± 40
C34 E119V β3,4-Ark1p + Abp1p	98 ± 15

Table S3. Experimental and fitted bound fractions for C34 WT.

[protein] (μM)	**[octapeptide] (μM)**	**G75 N-H^N**	**[a]N49 $N^{δ2}$-$H^{δ21}$**	**[a]N49 $N^{δ2}$-$H^{δ22}$**	**Fitted**
450	450	0.48 ± 0.03	0.47 ± 0.01	0.44 ± 0.02	0.49 ± 0.02
45	450	0.73 ± 0.09	0.76 ± 0.06	0.72 ± 0.08	0.64 ± 0.03
750	750	0.64 ± 0.03	0.67 ± 0.02	0.58 ± 0.03	0.58 ± 0.02

[a]$H^{δ21}$ and $H^{δ22}$ and are tentatively assigned based on reported chemical shift trends for δ21/δ22 protons (2)

Table S4. Experimental and fitted bound fractions for C34 Δβ4.

[protein] (μM)	**[octapeptide] (μM)**	**G75 N-H^N**	**N49 $N^{δ2}$-$H^{δ21}$**	**N49 $N^{δ2}$-$H^{δ22}$**	**Fitted**
450	450	0.73 ± 0.02	0.71 ± 0.01	0.67 ± 0.01	0.71 ± 0.02
45	450	0.93 ± 0.09	0.94 ± 0.05	0.89 ± 0.05	0.88 ± 0.02

Table S5. Experimental and fitted bound fractions for C34 E119V.

[protein] (μM)	**[octapeptide] (μM)**	**G75 N-H^N**	**N49 $N^{δ2}$-$H^{δ21}$**	**N49 $N^{δ2}$-$H^{δ22}$**	**Fitted**
450	450	0.04 ± 0.01	0.05 ± 0.01	0.05 ± 0.01	0.05 ± 0.01
45	450	0.10 ± 0.03	0.06 ± 0.02	0.05 ± 0.02	0.05 ± 0.01

Table S6. Experimental and fitted bound fractions for C34 E124RE.

[protein] (μM)	**[octapeptide] (μM)**	**V23 N-H^N**	**L65 N-H^N**	**L97 N-H^N**	**G105 N-H^N**	**Fitted**
450	450	0.37 ± 0.03	0.35 ± 0.01	0.31 ± 0.01	0.43 ± 0.01	0.41 ± 0.02
45	450	0.50 ± 0.09	0.56 ± 0.03	0.56 ± 0.03	0.57 ± 0.03	0.52 ± 0.03

Table S7. Experimental and fitted bound fractions for C34 E119V β3,4-Ark1p without the Abp1p SH3 domain.

[protein] (μM)	**[octapeptide] (μM)**	**G75 N-H^N**	**N49 $N^{δ2}$-$H^{δ21}$**	**N49 $N^{δ2}$-$H^{δ22}$**	**Fitted**
450	450	0.34 ± 0.02	0.34 ± 0.01	0.30 ± 0.01	0.36 ± 0.01
45	450	0.49 ± 0.04	0.50 ± 0.02	0.46 ± 0.02	0.42 ± 0.02

Table S8. Experimental and fitted bound fractions for C34 E119V β3,4-Ark1p with 1.3 fold excess Abp1p SH3 domain over C34.

[protein] (μM)	**[octapeptide] (μM)**	**[Abp1p] (μM)**	**G75 N-H^N**	**N49 $N^{\delta 2}$-$H^{\delta 21}$**	**N49 $N^{\delta 2}$-$H^{\delta 22}$**	**Fitted**
450	450	600	0.63 ± 0.04	0.61 ± 0.03	0.58 ± 0.03	0.63 ± 0.02
45	450	60	0.84 ± 0.06	0.83 ± 0.03	0.82 ± 0.04	0.81 ± 0.02

References

1. J. A. Marsh, V. K. Singh, Z. Jia, J. D. Forman-Kay, Sensitivity of secondary structure propensities to sequence differences between α- and γ-synuclein: Implications for fibrillation. *Protein Sci.* **15**, 2795–2804 (2006).
2. D. S. Wishart, C. G. Bigam, A. Holm, R. S. Hodges, B. D. Sykes, 1H, 13C and 15N random coil NMR chemical shifts of the common amino acids. I. Investigations of nearest-neighbor effects. *J. Biomol. NMR* **5**, 67–81 (1995).